

Research on stroke medical image classification based on Wavelet Scattering Network

Zhongying Pei^{1*}, Zhoule Pei²

¹College of Electronic and Communication Engineering, Tianjin Normal University, Tianjin, China

²College of Information and Management Science, Henan Agricultural University, Zhengzhou, China

*Corresponding Author. Email: pzyTJNU@163.com

Abstract. Stroke can lead to brain dysfunction and, in severe cases, may result in long-term paralysis, aphasia, or memory impairment, significantly affecting daily life. Acute stroke episodes can be life-threatening and require timely treatment to minimize sequelae. Traditional stroke detection methods are often insensitive to early subtle lesions, prone to misdiagnosis or missed diagnosis, and incapable of real-time dynamic monitoring of disease progression. To overcome these limitations, this study proposes a stroke medical image classification method based on the Wavelet Scattering Network (WSN), aiming to improve the detection of stroke lesions. The WSN classifies medical images through multi-scale wavelet transformation and hierarchical nonlinear operations. The core principle involves first decomposing the image using wavelet filters to extract local features such as multi-scale edges and textures. This is followed by modulus operations to eliminate phase variations and enhance translation invariance, and then layer-by-layer downsampling to compress feature dimensions. Finally, stable low-dimensional feature vectors are generated for classification. The proposed method was applied to Dataset 1 and the stroke dataset from the Teknofest-2021 Medical AI Competition. The results show that the method achieved an accuracy of 88.69% on Dataset 1 and 93.75% on the Teknofest-2021 dataset. Compared with traditional methods such as Convolutional Neural Networks (CNN) and Long Short-Term Memory Networks (LSTM), the proposed approach improves classification accuracy by 7.33%–11.33%. The WSN-based method effectively overcomes the limitations of traditional stroke medical image classification and diagnosis techniques, offering a novel technical approach and solution for this field.

Keywords: stroke, WSN, medical image, multi-scale wavelet transform, classification accuracy

1. Introduction

Stroke is the second leading cause of death globally and the primary cause of long-term disability among adults. Its high disability rate and complex sequelae not only lead to a severe decline in patients' quality of life but also impose a substantial medical and economic burden on families and society. According to the latest data from the World Health Organization and the Global Burden of Disease Study, there are approximately 110 million stroke survivors worldwide, with around 13.7 million new cases annually. Moreover, with the accelerating pace of population aging and the increasing burden of metabolic diseases, the global incidence of stroke is projected to rise by 34% by 2030, presenting a daunting challenge for prevention and control [1]. Therefore, achieving accurate detection of stroke is of great significance for early prevention and timely treatment.

Traditional stroke detection methods primarily include electroencephalogram (EEG) [2], neurological function assessment [3], and ultrasound examination [4]. EEG utilizes multi-angle X-ray beams to penetrate the skull and reconstruct cross-sectional images through computer processing, enabling rapid differentiation between cerebral hemorrhage (high-density shadows) and ischemic infarction (low-density lesions). However, this method has limited resolution in detecting small infarcts or posterior fossa lesions and poses a risk of radiation exposure. Neurological function assessment employs the National Institutes of Health Stroke Scale (NIHSS), which quantifies stroke severity through 11 clinical evaluations (such as consciousness, visual fields, facial palsy, and limb motor function). Nonetheless, its accuracy is highly dependent on physicians' expertise and is less sensitive to posterior circulation strokes. Ultrasound examination detects carotid plaques, stenosis, and changes in intracranial hemodynamics via ultrasound waves to assess stroke risk. However, this approach is highly operator-dependent and has limited capacity to visualize distal vascular lesions. To address the limitations of these methods, this study adopts a medical image-based approach for stroke detection. Compared with traditional techniques, medical imaging offers significant advantages in

objectivity, resolution, and lesion visualization. Unlike EEG, which has limited spatial resolution and only indirect correlations with brain function, medical imaging can directly localize structural abnormalities. Compared with the subjectivity and delayed symptom presentation of neurological assessments, image analysis can reveal subtle pathological changes at early stages. Furthermore, in contrast to the acoustic window limitations and operator dependence of ultrasound, multimodal imaging technologies—such as perfusion imaging—can comprehensively quantify cerebral hemodynamic parameters. When combined with artificial intelligence algorithms, these technologies enable rapid, accurate, and automated diagnosis, providing highly reliable and visualized evidence to support clinical decision-making [5].

In recent years, deep learning models have been widely applied in the field of medical image classification. Examples include Convolutional Neural Networks (CNN) [6], Residual Networks with Convolutional Block Attention Modules (ResNet-CBAM) [7], Vision Transformers (ViT) [8], and Visual Geometry Group Networks (VGG) [9], among others. For instance, Gautam et al. proposed a method combining image fusion and CNN. By employing multi-focus image fusion as a preprocessing step to enhance the quality of CT images, they conducted two experiments on different datasets to validate the approach. The results showed classification accuracies of 98.33% on Dataset 1 and 98.77% in the second experiment [10]. However, this method demonstrates several limitations in medical image processing, including strong dependence on data, limited generalization capability, and a lack of interpretability. Tahyudin et al. proposed the ResNet-CBAM model, which integrates a residual network architecture with a convolutional block attention module to enhance the detection of critical features in CT images. The results indicated that the model achieved a classification accuracy of 95% for distinguishing normal from stroke images, with precision, recall, and F1 scores all exceeding 93% for stroke and non-stroke categories [11]. While ResNet-CBAM improves feature detection performance, the introduction of attention modules increases computational cost and necessitates a larger volume of training data; otherwise, the model is prone to overfitting under small-sample conditions. Yopiangga et al. employed CT scan images and the ViT method. By preprocessing patient CT images and segmenting them to localize key regions, classification efficiency was improved. Based on the pretrained Vision Transformer Base-16 model and after parameter optimization, the approach achieved a test accuracy of 91% on the stroke classification task [12]. Nevertheless, the method's heavy reliance on large-scale labeled datasets, high computational complexity resulting in substantial resource consumption, and lack of prior knowledge of local features may lead to omission of subtle lesion details in medical image analysis. Sakinah et al. proposed a method based on the VGGNet-16 architecture. After enhancing CT image quality during preprocessing, a CNN model based on the VGGNet-16 structure achieved a training accuracy of 99.62% and a test accuracy of 99.5% in stroke classification, following parameter optimization. However, this method faces issues such as high computational cost, risk of overfitting, and insufficient sensitivity of deep networks to subtle lesions in medical images, making it difficult to adaptively optimize the expression of local features [13].

To address the limitations of the aforementioned methods, this study proposes the use of a Wavelet Scattering Network (WSN) for the classification of stroke CT images. Compared with traditional deep learning models such as CNN, ResNet-CBAM, ViT, and VGG, WSN exhibits distinct advantages in medical image classification. Its predefined filter bank based on wavelet transforms enables multi-scale and multi-directional geometric feature extraction, significantly reducing dependence on large-scale annotated datasets and mitigating the risk of overfitting caused by redundant parameters in CNN and VGG models. In contrast to the computational complexity introduced by the attention mechanisms in ResNet-CBAM, WSN achieves rotational and translational invariance through mathematically modeled hierarchical scattering paths, allowing it to stably characterize morphological features of lesions even in the presence of noise interference [14]. Furthermore, unlike ViT, which requires massive datasets to support global modeling via self-attention, WSN is capable of efficiently capturing subtle pathological changes—such as early ischemic diffusion abnormalities—even under limited sample conditions, as is common in small-scale stroke datasets. In addition, WSN offers theoretical interpretability, making it a robust, low-cost, and tuning-free solution for medical image classification.

2. Dataset

2.1. Stroke dataset

The dataset used in this study was compiled from the clinical Picture Archiving and Communication System (PACS) records of three institutions: Stanford University (Palo Alto, California, USA), the Federal University of São Paulo (São Paulo, Brazil), and Thomas Jefferson University Hospital (Philadelphia, Pennsylvania, USA) [15]. It includes annotated head CT scans representing five common subtypes of intracranial hemorrhage: subarachnoid hemorrhage, intraventricular hemorrhage, subdural hemorrhage, epidural hemorrhage, and intraparenchymal hemorrhage. The total number of images amounts to 874,035. The dataset was curated using label distributions from each contributing site to standardize exam distributions in the merged testing and validation sets. Data from each institution was partitioned into cohorts of 500 examinations, with the last 100 examinations from each cohort selected for the testing and validation sets. These were independently reviewed by two additional neuroradiologists. Fifteen percent of the triple-reviewed examinations were used for the final test set, while the remaining 5% were used for

validation. Each series in the final dataset contains between 20 and 60 axial images with slice thicknesses ranging from 3 to 5 mm. After the curation process, the final dataset comprised 25,312 examinations, of which 21,784 were used for training and validation, and 3,528 for testing. Although this use case successfully captures the intended complexity and heterogeneity, it required a substantial amount of expert manual annotation. The dataset is publicly available on RSNA under the CC-BY-NC 4.0 license. Users must sign a data usage agreement and provide proper citation. Dataset access link: <http://pubs.rsna.org/doi/full/10.1148/ryai.2020190211>

2.2. Teknofest-2021 stroke dataset

This dataset originates from the Teknofest-2021 Medical Artificial Intelligence Competition: Stroke Dataset, which contains anonymized head computed tomography (CT) images [16]. The dataset was curated, compiled, and annotated by seven radiologists. For the planned training and testing datasets, data recorded during 2019 and 2020 were centrally filtered using various codes and selection criteria from the e-Pulse system and the Remote Radiology System of the Ministry of Health of the Republic of Türkiye. To construct the dataset, a total of 877 CT and 230 MRI studies were collected from 819 unique cases. The final training dataset consists of 6,651 images: 4,427 images show no evidence of stroke, chronic ischemic findings, or contain only normal findings; 1,131 images exhibit hyperacute/acute ischemic stroke findings; and 1,093 images show hemorrhagic stroke findings. The dataset preparation was organized by the Ministry of Health of the Republic of Türkiye. This study received ethical approval from the Ministry, and informed consent was waived due to the retrospective analysis of anonymized data from the national health database. Dataset access link: <https://pmc.ncbi.nlm.nih.gov/articles/PMC9797774/>

3. Method

3.1. Wavelet scattering transform

The wavelet transform involves convolving a signal with a set of wavelet families obtained by rotating and scaling a mother wavelet, thereby generating wavelet feature coefficients [17]. Specifically, let $\psi_{j,\gamma}(u) = 2^{-2j}\psi_\gamma(2^{-j}u)$ be the directional mother wavelet function, where γ denotes direction and j denotes scale; let $\phi_J(u) = 2^{-2J}\phi(2^{-J}u)$ represent the scaling function at the maximum scale J . Then, the wavelet transform is defined as Equation (1):

$$W_J f = \{A_J f, W_{j,\gamma} f\}_{j < J} \quad (1)$$

In Equation (1), $W_{j,\gamma} f(x) = f^* \psi_{j,\gamma}(x)$ represents the high-frequency information at scale j and direction γ . $A_J f = f^* \phi_J$ represents the low-frequency information at the maximum scale J . Therefore, the wavelet transform produces a set of wavelet feature coefficients $\{W_{j,\gamma} f\}_{j \leq J}$ across different directions and scales. Due to the local deformation, scale, and rotational invariance properties of the wavelet coefficients, they are commonly applied in processing images, speech, and other signals that can be transformed into the time-frequency domain. However, wavelet coefficients are sensitive to local translations and thus do not possess translation invariance.

Wavelet scattering applies a modulus operation to the wavelet transform coefficients primarily because the mean of the wavelet coefficients is zero. After linear transformation, the mean remains zero; therefore, by applying a nonlinear operation (taking the modulus), a non-zero wavelet coefficient is obtained, enabling it to carry meaningful information.

The modulus of the wavelet transform is defined as Equation (2):

$$U_\lambda f(x) = |f^* \psi_\lambda(x)| \quad (2)$$

At this stage, the wavelet features, which have undergone nonlinear operations, are convolved with the scaling function for averaging (low-pass filtering) to obtain wavelet features that possess both translation invariance and stability to local deformations, as shown in Equation (3):

$$S_j(\lambda) f = |f^* \psi_\lambda(x)|^* \phi_j \quad (3)$$

Equation (3) is also referred to as the wavelet scattering transform.

3.2. Wavelet scattering representation

After the signal undergoes the wavelet scattering transform, the averaging operation makes the wavelet feature coefficients relatively stable; however, it also suppresses high-frequency components, resulting in some information loss and reducing the discriminative power of the wavelet feature coefficients. To recover high-frequency information, the wavelet modulus can be further decomposed at relatively larger scales (which must be smaller than the maximum scale). Nevertheless, these features still lack translation invariance, so further modulus operations and averaging (low-pass filtering) are required to achieve stability of the feature coefficients. This process is illustrated in Equation (4):

$$S[\lambda_1, \lambda_2]f = (|f * \psi_{\lambda_1}(x)| * \psi_{\lambda_2}(x)) * \phi_j \tag{4}$$

In Equation (4), where $\lambda_1 < \lambda_2 < J$.

Each averaging of features is accompanied by the loss of high-frequency information. Therefore, to ensure energy conservation, it is necessary to iteratively apply the wavelet scattering transform to the coefficients from the previous layer. Consequently, the obtained wavelet scattering feature coefficients are expressed as shown in Equation (5):

$$S[\lambda_1, \dots, \lambda_n]f = (\dots ((|f * \psi_{\lambda_1}(x)| * \psi_{\lambda_2}(x)| * \psi_{\lambda_3}(x)| \dots * \psi_{\lambda_n}(x)| * \phi_j \tag{5}$$

In Equation (5), where $\lambda_1 < \lambda_2 < \dots < \lambda_n < J$.

This process can be illustrated as shown in Figure 1:

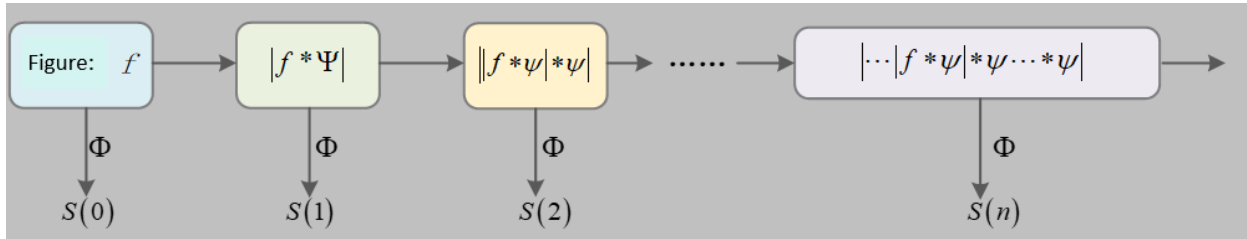


Figure 1. Propagation diagram of a signal through wavelet scattering

The propagation process begins with the input signal f . At each layer, after applying the wavelet transform modulus followed by convolution with the scaling function for averaging to extract features, the wavelet modulus is convolved with higher-frequency filters from the previous layer to recover the high-frequency components lost in the preceding layer. Therefore, each layer produces two outputs: one is the wavelet scattering feature coefficient $S_j(\lambda)f$, obtained by convolution with a low-pass filter, which yields a stable signal; the other is the wavelet transform modulus $U_\lambda f$, serving as the input for the next layer. To recover the lost high-frequency information, $U_\lambda f$ is further decomposed using higher-frequency filters at relatively larger scales. These two outputs can be expressed by Equation (6):

$$\overline{U_\lambda f} = \{U_\lambda f, S_j(\lambda)f\} = \{|f * \psi_\lambda|, |f * \psi_\lambda| * \phi_\lambda\} \tag{6}$$

Equation (6) is also referred to as the wavelet scattering propagation operator.

The signal is iteratively processed layer by layer, resulting in a series of scattering coefficient features $\{S(0), S(1), \dots, S(n)\}$.

3.3. Wavelet scattering algorithm

3.3.1. Wavelet scattering network structure

Wavelet scattering can be described as the process where the original signal is filtered by wavelet filters to obtain high-frequency and low-frequency information. The low-frequency information corresponds to the desired features, but these features require nonlinear and stationary transformations to ensure invariance to signal deformations [18]. Meanwhile, the high-frequency information can be further processed to extract additional features. This process of wavelet transform followed by nonlinear transformation is repeated iteratively, continuously extracting features from the original signal.

Let the scattering path be $P = \{\lambda_1, \lambda_2, \lambda_3, \dots, \lambda_m\}$, where m denotes the maximum path length. Accordingly, scattering feature coefficients of orders from 1 to m , denoted as $\{S_j[\phi]f, S_j[\lambda_1]f, \dots, S_j[\lambda_1, \dots, \lambda_m]f\}$, can be obtained. Based on Section 3.2, the wavelet scattering convolutional neural network is illustrated in Figure 2 as follows:

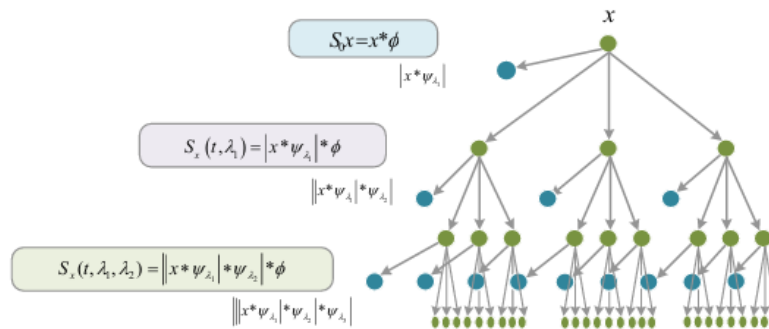


Figure 2. Wavelet scattering convolutional neural network

The network structure of wavelet scattering is shown in the figure above. The output of each layer in the network corresponds to the extracted features, referred to as the wavelet scattering transform. The feature coefficients can be expressed by Equation (7):

$$S_j \begin{bmatrix} P_j \end{bmatrix} f = \begin{pmatrix} S_j[\phi]f \\ S_j[A_j^1]f \\ S_j[A_j^2]f \\ S_j[A_j^3]f \\ \vdots \end{pmatrix} = \begin{pmatrix} f * \varphi_{2^j} \\ |f * \psi_{\lambda_1}| * \varphi_{2^j} \\ ||f * \psi_{\lambda_1}| * \psi_{\lambda_2}| * \varphi_{2^j} \\ |||f * \psi_{\lambda_1}| * \psi_{\lambda_2}| * \psi_{\lambda_3}| * \varphi_{2^j} \\ \vdots \end{pmatrix}_{\lambda_1, \lambda_2, \lambda_3, \dots} \quad (7)$$

Its network structure is similar to that of deep Convolutional Neural Networks (CNNs), as both obtain features of the original input through convolution kernels (linear transformations) followed by nonlinear transformations (modulus operation) layer by layer. However, there are key differences:

(1) The convolution kernels in wavelet scattering use predefined wavelet filters, which extract optimal features by rotating and scaling the mother wavelet. Therefore, the network contains no trainable weights, significantly reducing computational complexity. In contrast, deep CNNs require learning convolution kernels through feedback-based iterative computations, resulting in higher computational costs.

(2) In WSN, each layer produces feature outputs, and the final feature representation is formed by concatenating the outputs from all layers. Conversely, in deep CNNs, only the final layer's output serves as the feature descriptor for the object.

3.3.2. Wavelet scattering algorithm procedure

Based on the aforementioned WSN structure, the pseudo-code for the wavelet scattering transform algorithm is presented in Table 1 below:

Table 1. Wavelet scattering algorithm procedure

Step 1:	Input the image f .
Step 2:	Design the wavelet kernels according to the image size, then sequentially convolve the modulus output from the previous layer. Let $U_J(0)f = f$ for $m = 1: m_{max} - 1$ do For $j = 1: J - 1$ and $\gamma \in G$ do $S(j, \gamma)f = U_{j,\gamma}f * \phi_J$ $U_{j,\gamma}f = U_{j-1,\gamma} * \psi_{j,\gamma}$ end for end for
Step 3:	Obtain the final feature set according to the wavelet scattering results: S_Jf

3.4. Evaluation metrics

This study selects accuracy, precision, recall, and F1 score as the evaluation metrics for the WSN. The definitions of these four metrics are as follows [19]:

(1) Accuracy is the proportion of correctly predicted samples to the total number of samples, as shown in Equation (8):

$$Accuracy = \frac{TP + FN}{TP + FP + FN + TN} \quad (8)$$

(2) Precision is the proportion of true positive samples among those predicted as positive by the model, as shown in Equation (9):

$$Precision = \frac{TP}{TP + FP} \quad (9)$$

(3) Recall is the proportion of true positive samples correctly predicted by the model among all actual positive samples, as shown in Equation (10):

$$Recall = \frac{TP}{TP + FN} \quad (10)$$

(4) The F1 score is the harmonic mean of precision and recall, providing a comprehensive evaluation of model performance, as shown in Equation (11):

$$F1 \text{ score} = 2 \frac{Precision * Recall}{Precision + Recall} \quad (11)$$

In the above Equations (8) to (11), True Positives (TP) refer to samples predicted as positive that are actually positive. False Positives (FP) are samples predicted as positive but are actually negative. False Negatives (FN) are samples predicted as negative but are actually positive. True Negatives (TN) refer to samples predicted as negative that are actually negative.

4. Results

4.1. Classification results on dataset 1

This study selected stroke CT images provided by three institutions (Stanford University, Federal University of São Paulo, and Thomas Jefferson University). The images were annotated with five types of hemorrhagic symptoms: subarachnoid hemorrhage, intraventricular hemorrhage, subdural hemorrhage, epidural hemorrhage, and intracerebral hemorrhage. The dataset comprises a total of 874,035 images. The experiment was implemented using MATLAB 2020, with R as the programming language. The number of wavelet layers was set to 2, and the Marr wavelet was selected. The training and testing datasets were split at a ratio of 7:3. Classification was performed using a Support Vector Machine (SVM). The classification results are shown in Figure 3.

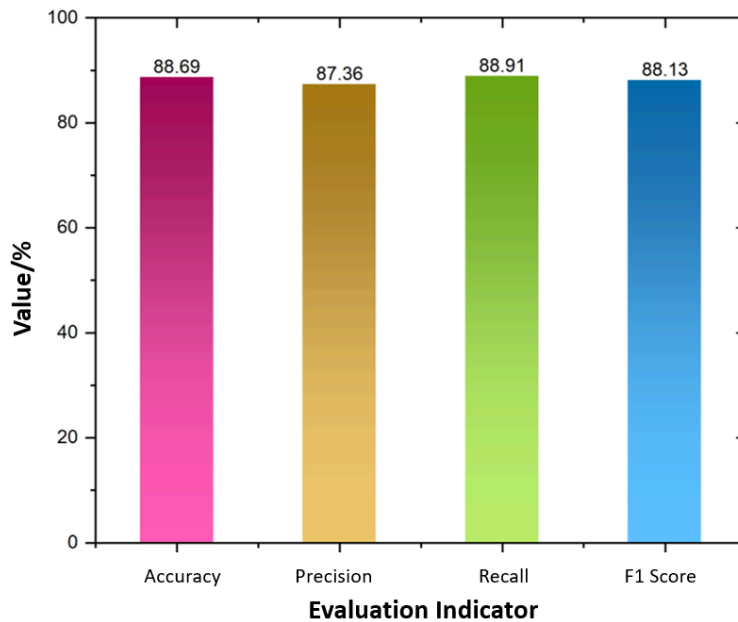


Figure 3. Classification results on dataset 1

As shown in Figure 3, the WSN method proposed in this study achieved an accuracy of 88.69%, precision of 87.36%, recall of 88.91%, and an F1 score of 88.13% in classifying the five types of stroke-related symptoms. The values of these metrics are relatively close, collectively indicating that the classification model performs well on this dataset.

4.2. Classification results on dataset 2

The stroke dataset consists of axial head Computed Tomography (CT) images, including a total of 6,653 brain CT slices. Among these, 4,428 images belong to the non-stroke category, 1,131 images to the ischemic stroke category, and 1,094 images to the hemorrhagic stroke category. In this study, the training and testing sets were divided at a ratio of 8:2. The implementation was carried out using MATLAB 2020, with R as the programming language. The classification results are presented in Table 2.

Table 2. Classification results on dataset 2

Evaluation Metric	Accuracy	Precision	Recall	F1 Score
Overall Value (%)	93.75	92.16	92.87	92.51

Table 2 presents the classification results of stroke recognition on Dataset 2 using the WSN method. The accuracy reached 93.75%, precision was 92.16%, recall was 92.87%, and the F1 score was 92.51%. These metrics demonstrate the strong performance of the proposed method in the task of stroke disease recognition.

5. Discussion

5.1. Comparison with other methods

To demonstrate the significant advantages of the proposed method in terms of accuracy and computational complexity, this study conducted a comparison on Dataset 1 using other traditional image classification methods, such as Convolutional Neural Networks (CNN) and Long Short-Term Memory networks (LSTM). The comparison results are presented in Table 3.

Table 3. Comparison between the proposed method and other methods

Method	Accuracy	Testing Time (ms)
CNN	77.36	86
long short-term memory, LSTM [20]	81.79	74
Graph neural network GCN [21]	84.72	67
Capsule Neural Network, CapsNet [22]	86.88	46
WSN (This study)	88.69	41

As shown in Table 3, when classifying stroke CT images using CNN, LSTM, GCN, CapsNet, and the proposed WSN method, WSN achieved the best performance with an accuracy of 88.69% and a testing time of 41 ms. This was followed by CapsNet with an accuracy of 86.88%. The accuracies of GCN, LSTM, and CNN were 84.72%, 81.79%, and 77.36%, respectively.

WSN possesses unique advantages in medical image classification. Its filters are predefined wavelet filters that do not require parameter learning from training samples, thus eliminating reliance on large-scale datasets and enabling strong performance even with small sample sizes [23]. Through semi-discrete wavelet transform and nonlinear modulus operations, WSN extracts signal features with desirable properties such as translation invariance and deformation stability. These properties are rigorously proven mathematically, addressing the theoretical gaps present in CNNs [24]. Moreover, compared to Long Short-Term Memory networks (LSTMs), which are primarily designed for sequence data and are less specialized in image classification, WSN focuses more directly on image feature extraction and classification. Compared to Graph Neural Networks (GCNs), WSN benefits from more mature theories and methods for fundamental image feature extraction. Relative to Capsule Networks (CapsNets), WSN avoids issues such as slow training and difficulties in recognizing certain scenarios, enabling more stable and efficient feature extraction and classification in medical image tasks.

5.2. Limitations and future prospects

Although WSN demonstrates significant advantages in overcoming the limitations of traditional methods in stroke medical image classification, certain limitations remain. For example, it may be less flexible and efficient than some deep neural networks in finely capturing complex lesion details and in multimodal data fusion. Additionally, there is room for further improvement in computational efficiency and real-time applicability of the model. Future research could explore deeper integration of WSN with other deep learning models, such as LSTM, to leverage complementary strengths and enhance the capacity for processing complex medical images. Investigations into optimizing network architectures to improve computational efficiency and better suit real-time dynamic monitoring scenarios are also warranted. Furthermore, enhancing the fusion of multimodal medical data combined with more clinical information could further improve classification accuracy and clinical utility, thereby providing stronger technical support for precise diagnosis and treatment of stroke.

6. Conclusion

This study proposes the application of the Wavelet Scattering Network (WSN) for the classification of stroke CT images, successfully overcoming the shortcomings of traditional detection methods, such as reduced sensitivity to early subtle lesions and high misdiagnosis rates. On a multicenter dataset containing five hemorrhage subtypes, WSN achieved an accuracy of 88.69% (precision 87.36%, recall 88.91%). On a three-class dataset (ischemic/hemorrhagic/normal, n=6653), the accuracy improved to 93.75% (F1 score 92.51%). Compared with benchmark models such as CNN and LSTM, WSN significantly improved accuracy by 7.33–11.33%, with a detection speed of 41 ms per case. Compared to other methods, including CNN and LSTM, this approach offers stronger theoretical robustness, higher efficiency with small samples, and clinical interpretability, providing a novel solution for stroke disease detection.

References

- [1] El-Hajj, M., Salameh, P., Rachidi, S., & Hosseini, H. (2016). The epidemiology of stroke in the Middle East. *European Stroke Journal*, 1(3), 180–198.
- [2] Wu, J., Srinivasan, R., Quinlan, E. B., Solodkin, A., Small, S. L., & Cramer, S. C. (2016). Utility of EEG measures of brain function in patients with acute stroke. *Journal of Neurophysiology*, 115(5), 2399–2405.
- [3] Nakling, A. E., Aarsland, D., Næss, H., Wollschlaeger, D., Fladby, T., Hofstad, H., & Wehling, E. (2017). Cognitive deficits in chronic stroke patients: Neuropsychological assessment, depression, and self-reports. *Dementia and Geriatric Cognitive Disorders Extra*, 7(2), 283–296.
- [4] Herzberg, M., Boy, S., Hölscher, T., Ertl, M., Zimmermann, M., Ittner, K. P., Pemmerl, J., Pels, H., Bogdahn, U., & Schlachetzki, F. (2014). Prehospital stroke diagnostics based on neurological examination and transcranial ultrasound. *Critical Ultrasound Journal*, 6, 1–13.
- [5] Mayya, V., Tummala, V., Reddy, C. U., Mishra, P., Boddu, R., Olivia, D., & Kamath, S. S. (2023). Applications of machine learning in diabetic foot ulcer diagnosis using multimodal images: A review. *IAENG International Journal of Applied Mathematics*, 53(3).
- [6] Gautam, A., & Raman, B. (2021). Towards effective classification of brain hemorrhagic and ischemic stroke using CNN. *Biomedical Signal Processing and Control*, 63, 102178.
- [7] Xiao, Y., Yin, H., Wang, S. H., Zhang, Y. D., Yang, J., Liu, C., Zhang, Y., Wang, Q., & Zhang, B. (2021). TRcC: Transferred ResNet and CBAM for detecting brain diseases. *Frontiers in Neuroinformatics*, 15, 781551.
- [8] Alam, A. M., Ahad, A., & Ahmed, S. (2024). Comparative analysis of brain stroke prediction using various pretrained CNN and ViT models. In *2024 IEEE International Conference on Computing, Applications and Systems (COMPAS)* (pp. 1–6). IEEE.
- [9] Lai, Y. L., Wu, Y. D., Yeh, H. J., Lee, C. Y., Wang, J. J., & Chiu, H. Y. (2022). Using convolutional neural network to analyze brain MRI images for predicting functional outcomes of stroke. *Medical & Biological Engineering & Computing*, 60(10), 2841–2849.
- [10] Gautam, A., & Raman, B. (2021). Towards effective classification of brain hemorrhagic and ischemic stroke using CNN. *Biomedical Signal Processing and Control*, 63, 102178.
- [11] Tahyudin, I., Prabuwo, A. S., Dianingrum, M., Pandega, D. M., Winarto, E., Nazwan, Rozak, R. A., Lestari, P., & Tikaningsih, A. (2024). ResNet-CBAM in medical imaging: A high-accuracy tool for stroke detection from CT scans. In *2024 8th International Conference on Information Technology, Information Systems and Electrical Engineering (ICITISEE)* (pp. 551–556). IEEE.
- [12] Yopiangga, A. P., Badriyah, T., Syarif, I., & Sakinah, N. (2024). Stroke disease classification using CT scan image with vision transformer method. In *2024 International Electronics Symposium (IES)* (pp. 436–441). IEEE.
- [13] Sakinah, N., Subhan, M., Saputri, T. B. B., Badriah, T., & Syarif, I. (2024). VGGNet-16 convolutional neural network for classification of stroke based on CT scan images. *International Conference on Applied Science and Technology on Engineering Science 2023 (iCAST-ES 2023)* (pp. 1138–1150). Atlantis Press.
- [14] Agboola, H. A., & Zacheus, J. E. (2023). Wavelet image scattering based glaucoma detection. *BMC Biomedical Engineering*, 5(1), 1.
- [15] Flanders, A. E., Prevedello, L. M., Shih, G., Halabi, S. S., Kalpathy-Cramer, J., Ball, R., Mongan, J. T., Stein, A., Kitamura, F. C., Lungren, M. P., Choudhary, G., Cala, L., Coelho, L., Mogensen, M., Morón, F., Miller, E., Ikuta, I., Zohrabian, V., McDonnell, O., Lincoln, C., Shah, L., Joyner, D., Agarwal, A., Lee, R. K., Nath, J., & RSNA-ASNR 2019 Brain Hemorrhage CT Annotators. (2020). Construction of a machine learning dataset through collaboration: The RSNA 2019 brain CT hemorrhage challenge. *Radiology: Artificial Intelligence*, 2(3), e190211.
- [16] Koç, U., Akçapınar Sezer, E., Alper Özkaya, Y., et al. (2022). Artificial intelligence in healthcare competition (TEKNOFEST-2021): Stroke data set. *Eurasian Journal of Medicine*, 54(3), 248–258.
- [17] Lin, C.-L. (2010). A tutorial of the wavelet transform. *NTUEE, Taiwan*, 21(22), 2.
- [18] Liu, Z., Yao, G., Zhang, Q., Zhang, J., & Zeng, X. (2020). Wavelet scattering transform for ECG beat classification. *Computational and Mathematical Methods in Medicine*, 2020(1), 3215681.
- [19] Islam, M. M., Akter, S., Rokunojjaman, M., Rony, J. H., & Amin, A. (2021). Stroke prediction analysis using machine learning classifiers and feature technique. *International Journal of Electronics and Communications Systems*, 1(2), 17–22.
- [20] Yu, Y., Parsi, B., Speier, W., Arnold, C., Lou, M., & Scalzo, F. (2019). LSTM network for prediction of hemorrhagic transformation in acute stroke. In *International Conference on Medical Image Computing and Computer-Assisted Intervention* (pp. 177–185). Cham: Springer International Publishing.
- [21] Huang, Z., & Yu, S. (2024). Intelligent diagnosis and treatment model of hemorrhagic stroke based on graph convolutional neural network. In *Proceedings of the 2024 International Conference on Smart Healthcare and Wearable Intelligent Devices* (pp. 108–114).
- [22] Maya, B. S., & Asha, T. (2017). Segmentation and classification of brain hemorrhage using U-net and CapsNet. *Journal of Seybold Report ISSN NO*, 2017(1533), 9211.
- [23] Shi, J., Zhao, Y., Xiang, W., Monga, V., Liu, X., & Tao, R. (2021). Deep scattering network with fractional wavelet transform. *IEEE Transactions on Signal Processing*, 69, 4740–4757.
- [24] Bruna, J., & Mallat, S. (2013). Invariant scattering convolution networks. *IEEE Transactions on Pattern Analysis and Machine Intelligence*, 35(8), 1872–1886.